



Measuring ASKAP's On-Dish Calibration Signal Level and its Impact on Beam Sensitivity

Aaron Chippendale, Charissa Button & Liroy Lourenco

ASKAP Commissioning and Early Science Memo 018

October 31, 2018

CSIRO Astronomy and Space Science
Cnr Vimiera & Pembroke Roads, Marsfield, NSW 2122, Australia
PO Box 76, Epping, NSW 1710, Australia
Telephone : +61 2 9372 4100
Fax : +61 2 9372 4310

Copyright and disclaimer

© 2017 CSIRO To the extent permitted by law, all rights are reserved and no part of this publication covered by copyright may be reproduced or copied in any form or by any means except with the written permission of CSIRO.

Important disclaimer

CSIRO advises that the information contained in this publication comprises general statements based on scientific research. The reader is advised and needs to be aware that such information may be incomplete or unable to be used in any specific situation. No reliance or actions must therefore be made on that information without seeking prior expert professional, scientific and technical advice. To the extent permitted by law, CSIRO (including its employees and consultants) excludes all liability to any person for any consequences, including but not limited to all losses, damages, costs, expenses and any other compensation, arising directly or indirectly from using this publication (in part or in whole) and any information or material contained in it.

Contents

| | |
|--|----|
| 1 Summary | 1 |
| 2 ASKAP's On-Dish Calibration System | 2 |
| 3 Estimating Calibration Signal Levels at the PAF LNA Inputs | 3 |
| 4 Experiments | 5 |
| 5 Results | 6 |
| 5.1 Validation of the System Model | 6 |
| 5.2 Calibration Noise Power for Different Antennas and Attenuator Values | 7 |
| 5.3 Equalising the ODC Power Levels Across the Antennas | 7 |
| 5.4 Impact of ODC Signal on Beam Sensitivity | 11 |
| 6 Conclusion and Further Work | 13 |

1 Summary

The Australian Square Kilometre Pathfinder (ASKAP) telescope uses external noise sources to maintain calibration of its phased-array-feed (PAF) beams. This memo describes how we set the on-dish calibration (ODC) signal level and assess its impact on PAF beam sensitivity. This work took place during the commissioning of ASKAP's ODC systems and produced a number of useful diagnostics for assessing their health and function.

Key results include:

- a technique for measuring the ODC signal level relative to the single-port system noise power at the PAF low-noise amplifier (LNA) inputs;
- a procedure for setting up the same ODC signal level on each ASKAP antenna;
- a variety of diagnostics for assessing ODC health and function;
- finding that the ODC noise contribution is effectively mitigated by the standard maximum signal-to-noise ratio (maxSNR) beam weight solution so long as the ODC noise is on during beamforming; and
- finding that the ODC noise should raise the T_{sys} of beams by less than 1% so long as the ODC noise is on during beamforming and is no stronger than 24% of the single-port system noise power at the LNA inputs.

An earlier exploration of the utility of the ODC system for PAF diagnostics and calibration can be found in (Dowson, 2017).

2 ASKAP's On-Dish Calibration System

ASKAP uses external noise sources to maintain calibration of PAF beams. Figure 2.1 shows a functional schematic of the on-dish calibration (ODC) system (Beresford et al., 2018) that is installed for each ASKAP antenna. Each reflector antenna has a dedicated broadband noise source co-located with its digital backend at the central site. The calibration noise is transported via radio frequency over fibre (RFoF) to a small antenna, mounted at the vertex of each paraboloidal reflector, that radiates the noise into the PAF.

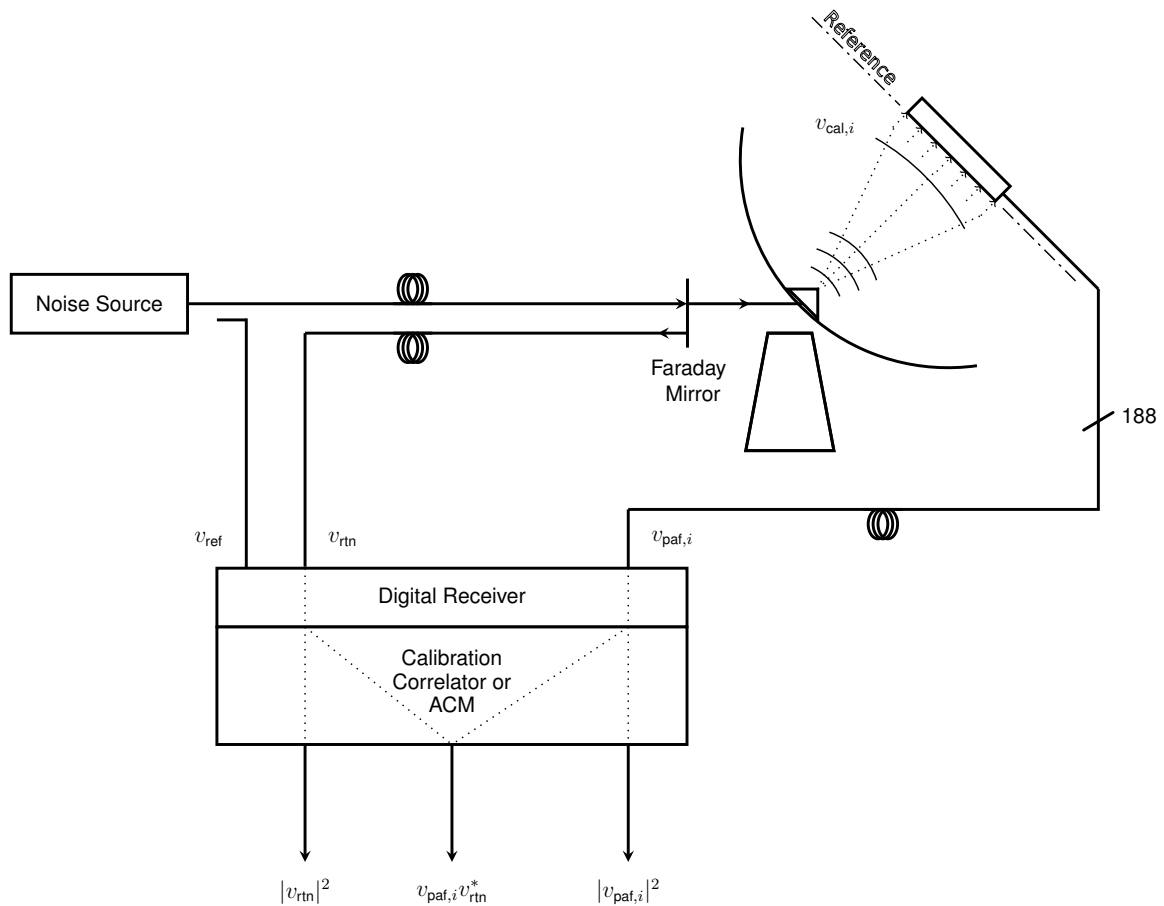


Figure 2.1: Schematic of the on-dish calibration (ODC) system.

There is a programmable attenuator to control the level of calibration noise radiated into the PAF. This may be set in 1 dB steps between 0 dB and 31 dB. Before this study it was common practice to set these values to a mid-range value of 16 dB by default.

Near the point where the calibration signal is converted back to an electrical signal for radiation into the PAF, a portion of the optical signal is reflected back along the fibre to the digital receiver (Brown et al., 2014) at the central site. This “return” copy v_{rtn} of the calibration signal travels a similar distance back to the digital receiver as the radiated signal $v_{cal,i}$ received at the i^{th} PAF port. A “reference” copy v_{ref} of the calibration signal is also directly injected into the digital receiver. This may be used in the future to extract the component of calibration corrections due to the RFoF link.

We used the Array Covariance Module (ACM), implemented in the firmware of ASKAP’s “Red-back” beamformer hardware (Hampson et al., 2014), to correlate the signals $v_{paf,i}$ received via

each PAF port with v_{rtn} . The correlations required for calibration are in the columns of the covariance matrix corresponding to v_{ref} and v_{rtn} . The firmware also includes a Calibration Correlator Module that calculates and downloads a single, user-specified column of the covariance matrix with up to 12.5% duty cycle. This is four times better than the best duty cycle possible for the full ACM download, making the Calibration Correlator twice as sensitive for estimating the response of the PAF to the ODC noise.

3 Estimating Calibration Signal Levels at the PAF LNA Inputs

To configure the calibration system, it is useful to estimate the level of calibration noise received at a given PAF port $v_{\text{cal},i}$ relative to the system noise power of that port $v_{\text{n},i}$. We define both of these quantities at a reference plane at the PAF low-noise amplifier (LNA) inputs, shown in Figure 2.1, and combine them with gain terms to make expressions for the signals received at the digital receiver and their correlations. Algebraic manipulations of these correlations yield the desired power ratio estimates.

The signal entering the digital receiver from the i^{th} PAF port can be expressed as

$$v_{\text{paf},i} = g_{\text{paf},i}(v_{\text{cal},i} + v_{\text{n},i}). \quad (3.1)$$

Here $v_{\text{cal},i}$ is the radiated calibration noise measured as a voltage at the input of the LNA on the i^{th} PAF port. $g_{\text{paf},i}$ is the complex-valued voltage gain from the input of that LNA via RFoF link back to the digital receiver input. Noise voltage $v_{\text{n},i}$ represents the end-to-end system noise of the i^{th} PAF port and its RFoF link, all referred to the LNA input.

The “return” copy of the calibration noise entering the digital receiver may be represented by

$$v_{\text{rtn}} = g_{\text{rtn}}v_{\text{cal},i} \quad (3.2)$$

where g_{rtn} is the complex-valued voltage gain of the “return” path of the calibration signal reflected back to the digital receiver. This gain is abstractly referred to the reference plane at the PAF LNA inputs. In (3.2) it is assumed that the calibration signal dominates any other instrumental noise at the digital receiver input. We also assume that no significant correlated noise is added at any point beyond the transmission of the calibration signal from the central site.

We now use (3.1) and (3.2) to expand the auto and cross-correlations of $v_{\text{paf},i}$ and v_{rtn} as

$$|v_{\text{paf},i}|^2 = |g_{\text{paf},i}|^2(|v_{\text{cal},i}|^2 + |v_{\text{n},i}|^2), \quad (3.3)$$

$$|v_{\text{rtn}}|^2 = |g_{\text{rtn}}|^2|v_{\text{cal},i}|^2, \text{ and} \quad (3.4)$$

$$v_{\text{paf},i}v_{\text{rtn}}^* = g_{\text{paf},i}g_{\text{rtn}}^*|v_{\text{cal},i}|^2. \quad (3.5)$$

These products are used to calculate the Pearson correlation coefficient

$$\begin{aligned} \rho &= \frac{v_{\text{paf},i}v_{\text{rtn}}^*}{\sqrt{|v_{\text{paf},i}|^2|v_{\text{rtn}}|^2}} \\ &= \frac{g_{\text{paf},i}g_{\text{rtn}}^*|v_{\text{cal},i}|^2}{|g_{\text{paf},i}|\sqrt{(|v_{\text{cal},i}|^2 + |v_{\text{n},i}|^2)}|g_{\text{rtn}}||v_{\text{cal},i}|} \\ &= \frac{e^{j(\theta_{\text{paf},i} - \theta_{\text{rtn}})}|v_{\text{cal},i}|}{\sqrt{|v_{\text{cal},i}|^2 + |v_{\text{n},i}|^2}} \end{aligned} \quad (3.6)$$

in which the gains have cancelled. Taking the absolute square of both sides gives

$$|\rho|^2 = \frac{|v_{\text{cal},i}|^2}{|v_{\text{cal},i}|^2 + |v_{\text{n},i}|^2} \quad (3.7)$$

which may be rearranged to

$$|\rho|^2 \left(\frac{|v_{\text{cal},i}|^2}{|v_{\text{n},i}|^2} + 1 \right) = \frac{|v_{\text{cal},i}|^2}{|v_{\text{n},i}|^2}. \quad (3.8)$$

Finally, we solve for the ratio of calibration power to system noise power at the input of a given PAF port

$$\frac{|v_{\text{cal},i}|^2}{|v_{\text{n},i}|^2} = \frac{|\rho|^2}{1 - |\rho|^2}. \quad (3.9)$$

Figure 3.1 shows violin plots of $10 \log_{10} (|v_{\text{cal},i}|^2/|v_{\text{n},i}|^2)$ evaluated via (3.9) for ASKAP scheduling block SB04768 during which all calibration noise attenuators were set to 16 dB. This figure summarises the calibration noise power level at the PAF LNA inputs for all 16 ASKAP antennas available at the time of measurement. The width of each “violin” shows an estimate of the probability density function of the power ratio from measurements of all 188 PAF ports and 336 one-megahertz frequency channels on one ASKAP antenna.

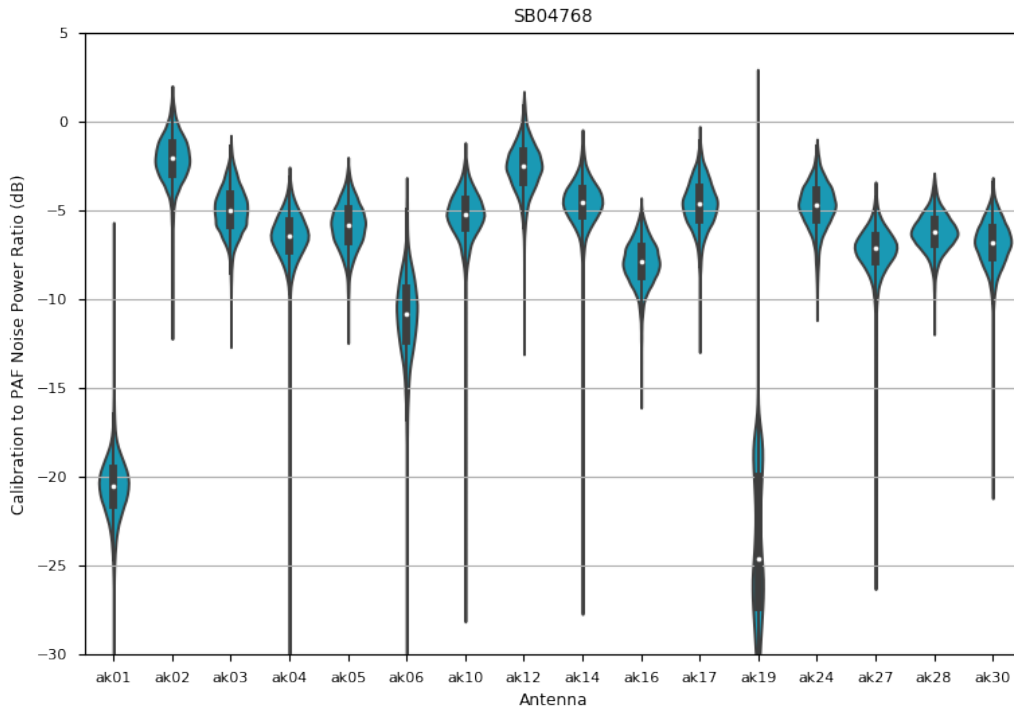


Figure 3.1: Power ratio between calibration and PAF noise at LNA inputs. The width of each “violin” shows an estimate of the probability distribution of the power ratio calculated from measurements of all 188 PAF ports and 336 one-megahertz frequency channels for a given ASKAP antenna. Measured via SB04768 on 27 November 2017. ODC attenuators were all set to 16 dB.

The very low power ratios for ak01 and ak19 suggest that their ODC systems were not working at the time of the measurement. The large negative ranges of outliers on antennas ak04, ak06, ak10, ak14, ak27 and ak30 suggest that some PAF ports have poor RF transmission through to the digital receiver on these antennas. Partitioning plots over polarisation and PAF port number would help to trace these problems, but is beyond the scope of the current work.

4 Experiments

Beyond the first single-shot measurement in SB04768 with default attenuator values, used for Figure 3.1, we performed three experiments that included coordinated sweeping of the attenuator values, formation of beams, and assessment of the sensitivity of beams with and without the ODC noise enabled.

Table 4.1 summarises the measurements involved in each experiment. Each scheduling block involved collecting ACMs from all available antennas while they tracked the Sun with a variety of offsets corresponding to a desired pattern of beams on the sky that we call the footprint. We used a single-beam `boresight` footprint in measurements targeted at understanding the impact of ODC noise on beam sensitivity as a function of the ODC power level. We used a 36-beam `square_6x6` footprint, that is typically used in ASKAP's imaging observations, to assess the impact of ODC noise on PAF beam sensitivity as a function of beam pointing within the PAF field of view (FOV). All beams used maximum signal-to-noise ratio (maxSNR) beamformer weights calculated according to McConnell et al. (2016).

Experiment 1 Boresight measurements with ODC off, then repeated with the ODC at two power levels separated by 10 dB. The aim was to quickly validate the derivations in Section 3, to see that our estimate of the power ratio from (3.9) changes by 10 dB for a controlled 10 dB change of the ODC power level.

Experiment 2 Sweep of the ODC attenuators over their full range whilst performing ACM measurements towards and away from the Sun at boresight. This was followed by two full `square_6x6` beamforming calibration measurement on the Sun: (1) with the ODC noise power at a relatively high level and (2) with the ODC noise turned off. The aim here was to measure impact of the ODC noise level on boresight beam performance, then at one particular ODC noise level, measure impact over the full FOV.

Experiment 3 Boresight measurements to determine per-antenna adjustments of the ODC attenuators so that the same radiated ODC noise power level is received by each ASKAP PAF. This was followed by a boresight measurement with the selected attenuator settings and another with 10 dB more power than the selected settings. Finally, a `square_6x6` beamforming calibration measurement was made with the higher power level setting to assess impact over the full FOV.

Table 4.1: Summary of experimental data. Antennas for which the ODC system was fully working at the time are shown in green. Numerical values indicate ODC RF attenuator value and “off” indicates that the ODC system was completely turned off.

| Scheduling block | ak01 | ak02 | ak03 | ak04 | ak05 | ak06 | ak10 | ak12 | ak14 | ak16 | ak19 | ak24 | ak27 | ak28 | ak30 | Beam |
|--------------------------------|------|------|------|------|------|------|------|------|------|------|------|------|------|------|------|-----------|
| Experiment 1 05/12/2017 | | | | | | | | | | | | | | | | |
| SB04788 | | | | Off | Off | | Off | Off | Off | | | Off | | | | Boresight |
| SB04789 | | | | 16 | 16 | | 16 | 16 | 16 | | | 16 | | | | Boresight |
| SB04790 | | | | 6 | 6 | | 6 | 6 | 6 | | | 6 | | | | Boresight |
| Experiment 2 10/01/2018 | | | | | | | | | | | | | | | | |
| SB04951 | 16 | 16 | 16 | 16 | 16 | 16 | 16 | 16 | 16 | | | 16 | 16 | 16 | 16 | Boresight |
| SB04952 | 0 | 0 | 0 | 0 | 0 | 0 | 0 | 0 | 0 | | | 0 | 0 | 0 | 0 | Boresight |
| SB04953 | 4 | 4 | 4 | 4 | 4 | 4 | 4 | 4 | 4 | | | 4 | 4 | 4 | 4 | Boresight |
| SB04954 | 8 | 8 | 8 | 8 | 8 | 8 | 8 | 8 | 8 | | | 8 | 8 | 8 | 8 | Boresight |
| SB04955 | 12 | 12 | 12 | 12 | 12 | 12 | 12 | 12 | 12 | | | 12 | 12 | 12 | 12 | Boresight |
| SB04956 | 16 | 16 | 16 | 16 | 16 | 16 | 16 | 16 | 16 | | | 16 | 16 | 16 | 16 | Boresight |
| SB04957 | 20 | 20 | 20 | 20 | 20 | 20 | 20 | 20 | 20 | | | 20 | 20 | 20 | 20 | Boresight |
| SB04958 | 24 | 24 | 24 | 24 | 24 | 24 | 24 | 24 | 24 | | | 24 | 24 | 24 | 24 | Boresight |
| SB04959 | 28 | 28 | 28 | 28 | 28 | 28 | 28 | 28 | 28 | | | 28 | 28 | 28 | 28 | Boresight |
| SB04960 | 31 | 31 | 31 | 31 | 31 | 31 | 31 | 31 | 31 | | | 31 | 31 | 31 | 31 | Boresight |
| SB04961 | 16 | 16 | 16 | 16 | 16 | 16 | 16 | 16 | 16 | | | 16 | 16 | 16 | 16 | Boresight |
| SB04962 | 6 | 6 | 6 | 6 | 6 | 6 | 6 | 6 | 6 | | | 6 | 6 | 6 | 6 | 6x6 beam |
| SB04963 | Off | | | Off | Off | Off | Off | Boresight |
| SB04964 | Off | | | Off | Off | Off | Off | 6x6 beam |
| Experiment 3 11/01/2018 | | | | | | | | | | | | | | | | |
| SB04974 | 16 | 16 | 16 | 16 | 16 | 16 | | 16 | 16 | 16 | 16 | 16 | | | | Boresight |
| SB04975 | 0 | 24 | 18 | 0 | 17 | 6 | | 23 | 19 | 13 | 0 | 18 | | | | Boresight |
| SB04976 | 0 | 24 | 18 | 0 | 17 | 13 | | 23 | 19 | 13 | 0 | 18 | | | | Boresight |
| SB04977 | 0 | 24 | 18 | 0 | 17 | 10 | | 23 | 19 | 13 | 0 | 18 | | | | Boresight |
| SB04979 | 18 | 24 | 18 | 18 | 17 | 10 | | 23 | 19 | 13 | 18 | 18 | | | | Boresight |
| SB04980 | 8 | 14 | 8 | 8 | 7 | 0 | | 13 | 9 | 3 | 8 | 8 | | | | Boresight |
| SB04981 | 8 | 14 | 8 | 8 | 7 | 0 | | 13 | 9 | 3 | 8 | 8 | | | | 6x6 beam |

5 Results

5.1 Validation of the System Model

In experiment 1, scheduling blocks SB04789 and SB04790, with attenuator values of 16 dB and 6 dB respectively, were used to estimate the ratio of the calibration power to noise power via (3.9). From scheduling blocks SB04789 to SB04790, the ODC power level increased by 10 dB while the PAF noise power level did not change. Thus, the ratio of the ODC power to the receiver noise power should increase by 10 dB from SB04789 to SB04790.

We measured a power ratio of 10.0 ± 0.2 dB between the two scheduling blocks. This is the median and standard deviation of all power ratios calculated independently for each 1 MHz channel of each PAF port of each antenna with a working ODC system. As expected the ratio is very close to 10 dB. This suggests that the calibration to noise ratio in (3.9) is a useful quantity for estimating the power of the on-dish calibrator.

5.2 Calibration Noise Power for Different Antennas and Attenuator Values

In Experiment 2, the ODC attenuator values were increased in 4 dB steps covering the full range of attenuation. A measurement at the mid-range attenuation of 16 dB was made before and after the full sweep to check for any drift during the measurement. A final measurement was made with the ODC turned off so we could see how close the maximum attenuation scenario was to a completely absent ODC signal. We did this as the ODC noise sources have a relatively long power-up time constant that might be avoided by leaving them on all the time and switching to a high attenuation when we don't want to use them.

Figure 5.1 shows the measured calibration noise power received at the PAFs versus the SBID for two antennas with working ODC systems. The ODC attenuation setting for each measurement (SBID) can be looked up in Table 4.1. These results show that:

- The same ODC attenuator value yields different calibration noise powers at the PAF LNA input for different antennas. Although this is best illustrated by Figure 3.1.
- The same ODC attenuator value at later times yields the same calibration noise power at the PAF LNA input.
- The maximum attenuation is not equivalent to the ODC being off in terms of noise calibration power. Turning the ODC off reduces its power by at least a further 30 dB below the typical seen at the maximum attenuation value. A better strategy for avoiding the power-up time-constant might be to toggle the RFoF link that transports the noise signal to the antenna.

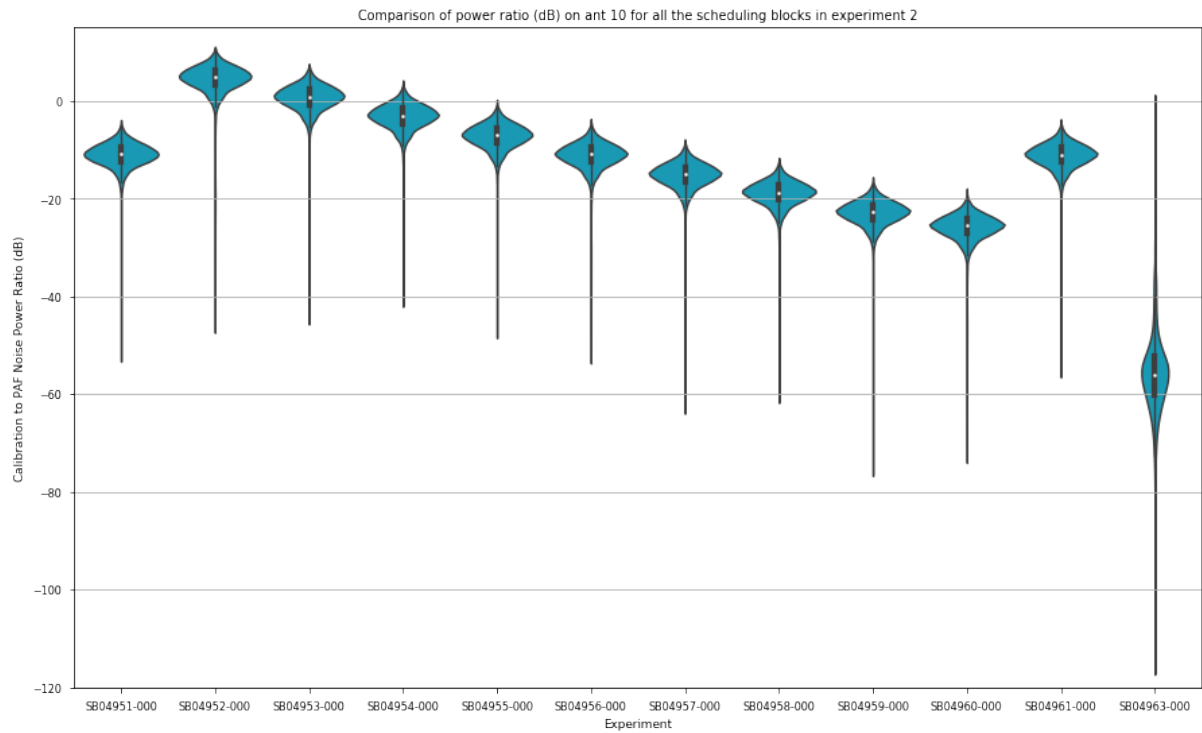
We expect that the median of the power ratio will decrease linearly with increasing attenuation. Figure 5.2, shows scatter plots for a selection of antennas with ODC systems in different states of repair. The expected trend was observed in all antennas with working ODC systems in Experiment 2: ak02, ak10, ak12 and ak30. Antenna 1 showed the correct trend, but was classed as not working as it had significantly lower ODC power levels than other working antennas.

A comparison of the calibration noise power with the attenuation level set to its maximum (31 dB) and with the ODC switched off, was performed. Figure 5.3 shows that, for antennas where the ODC is working, the received ODC power level is at least 30 dB lower when it is switched off than when the attenuator is at 31 dB.

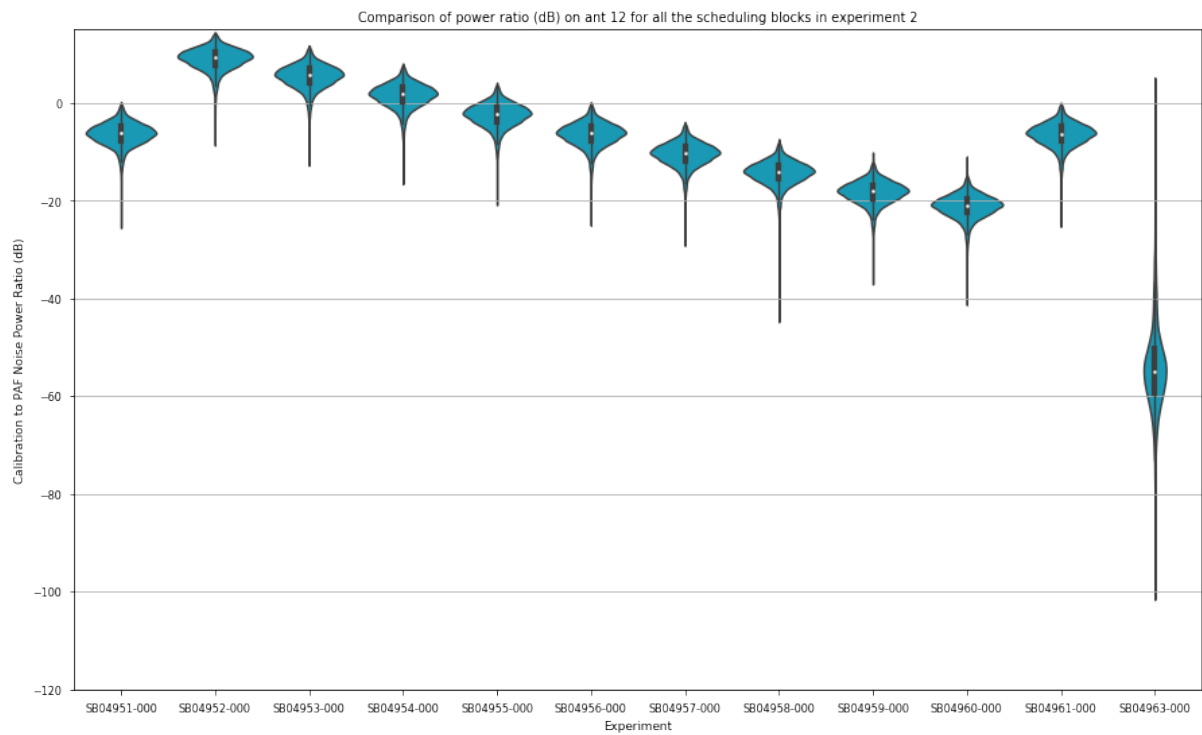
5.3 Equalising the ODC Power Levels Across the Antennas

Experiment 3 attempts to adjust the ODC attenuator values so that the radiated calibration noise power received at the PAF LNA inputs is approximately equal on all ASKAP antennas. See Table 4.1 for the attenuator values used. Figure 5.4 shows the ODC power levels after attempting align them. As before, the distributions for ak01, ak04, ak06 and ak19 indicated that their ODC systems were not functional. The inability to bring the ak02 calibration noise to the same level as other antennas, despite it having good noise power, suggested a misconnection of the noise source outputs at the central site, sending what should have been the direct reference signal out to the antenna and what should have been the signal for radiation directly into the digital receiver. This was confirmed by inspecting the amplitude of v_{ref} for ak02 and seeing that it varied linearly with the attenuation setting. For the remaining antennas, the calibration noise power distributions are more closely aligned.

Figure 5.5 shows a more recent attempt to align ODC powers across all 28 ASKAP antennas

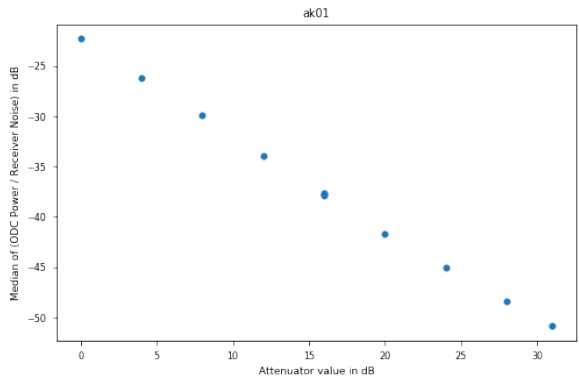


(a) Antenna 10

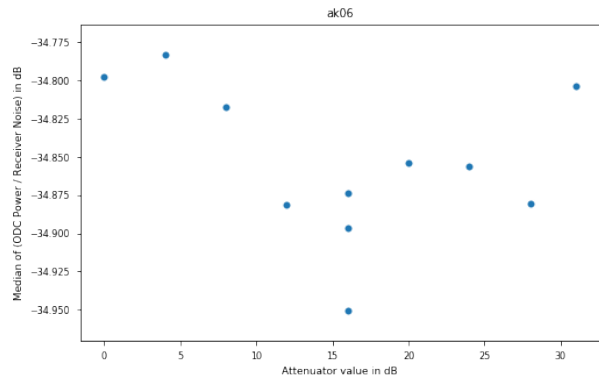


(b) Antenna 12

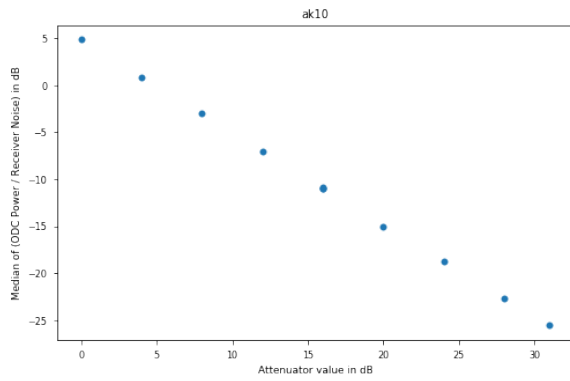
Figure 5.1: Calibration noise power levels at the PAF LNA inputs during the sweep of ODC attenuator values in Experiment 2. The first and penultimate measurements are of a mid-range attenuation of 16 dB and the final measurement is with the ODC system turned off.



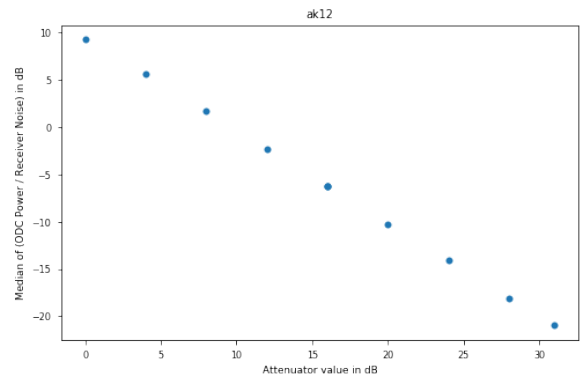
(a) Antenna 1 (low ODC power).



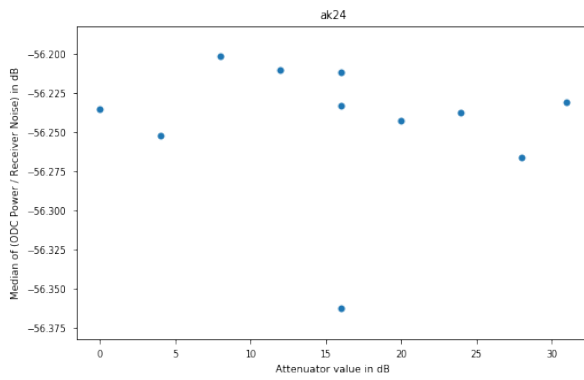
(b) Antenna 6 (faulty ODC).



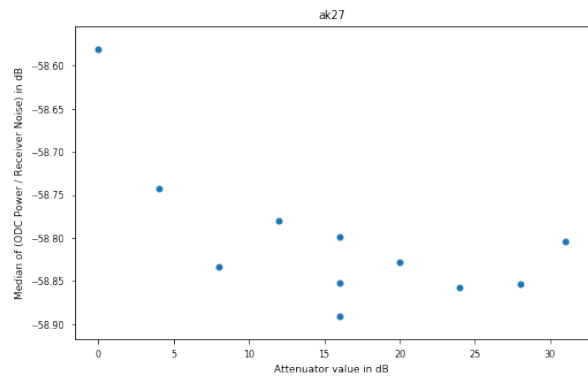
(c) Antenna 10.



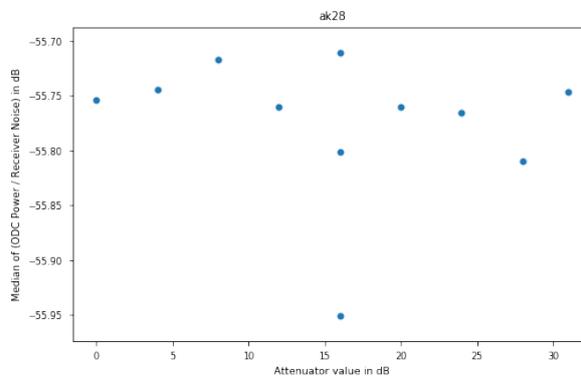
(d) Antenna 12.



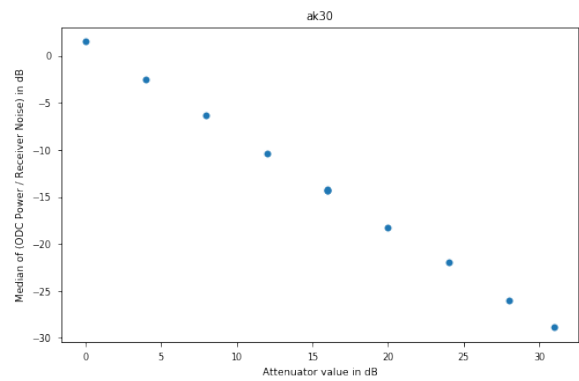
(e) Antenna 24 (faulty ODC).



(f) Antenna 27 (faulty ODC).



(g) Antenna 28 (faulty ODC).



(h) Antenna 30.

Figure 5.2: Median power ratio decreases linearly with attenuation on working antennas.

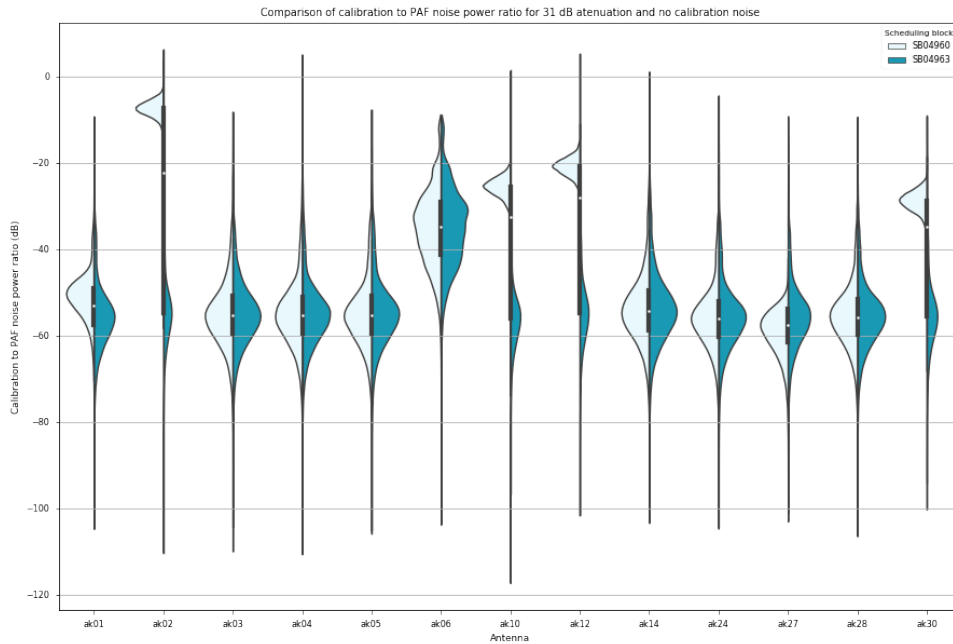


Figure 5.3: Comparison of 31 dB attenuation to the ODC being switched off, also clearly shows that ak02, ak10, ak12 and ak30 have operational ODCs and that the failure mode of the ODC on ak06 is different to that on other antennas with faulty ODCs.

available on 29 August 2018. The ODC power levels are equalised across all antennas except for, antenna ak01 which is low even with the attenuator set to zero, and antennas ak02, ak11, ak26, ak27, ak34 which were not working.

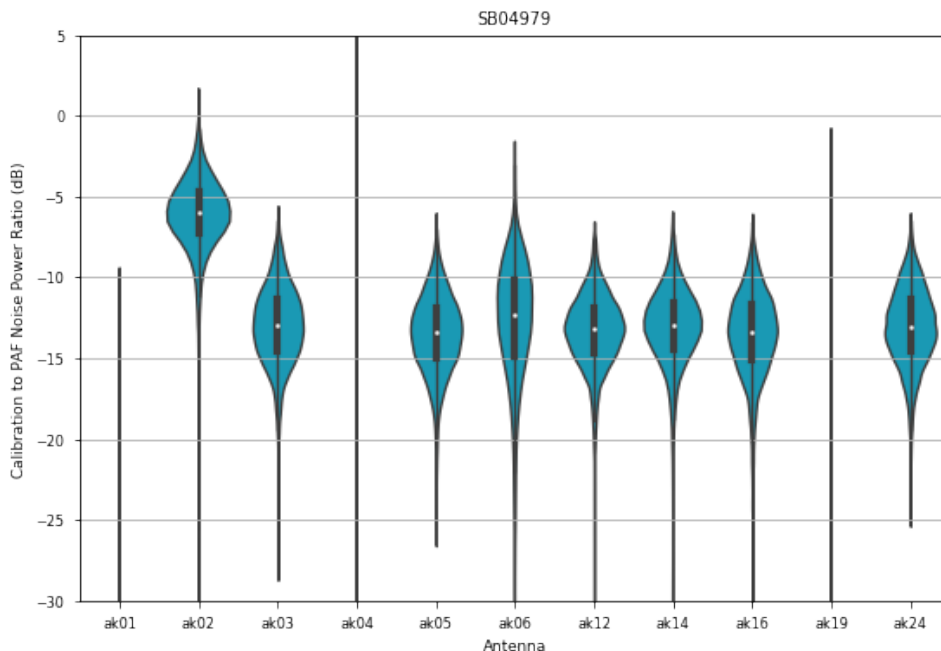


Figure 5.4: Calibration noise power ratio across all antenna in Experiment 3 after adjusting the RF attenuators. ODC power levels are aligned on all antennas except for ak02 which had mistakes in the cabling of its ODC system.

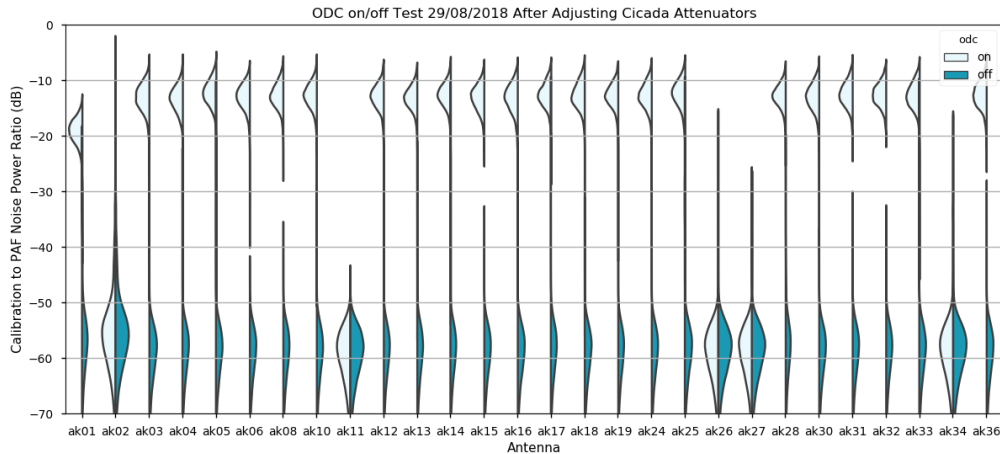


Figure 5.5: Recent calibration to PAF noise power ratio measurement comparing ODC on/off states across all 28 ASKAP antennas available on 29 August 2018. ODC attenuators were adjusted to equalise calibration noise across all antennas with working ODC systems.

5.4 Impact of ODC Signal on Beam Sensitivity

We assessed the impact of the ODC noise on beam sensitivity by computing the beamformed Y-Factor on the Sun. Figure 5.6 shows the Y-Factors for both polarisations for three scenarios: “matched” weights (blue) made and assessed with ODC on, “mismatched” weights (orange) made with ODC off and assessed with ODC on, and a reference “ODC off” case (red) where the ODC was off for both beamforming and sensitivity assessment.

Whether or not the noise source is on during beam weight calibration has a big impact. If the ODC is being used, significantly better sensitivity is obtained when the weights are determined with the noise on. This is because the maxSNR method tries to minimise all noise contributions, including the ODC noise when present, with respect to the desired signal. If the ODC is not turned on during beam weight calibration, it results in beams that are much more susceptible to contamination by the ODC noise.

Figure 5.6 also shows strong frequency structure in the Y-factor of the “mismatched” scenario where the ODC was turned off during beamforming then turned on for Y-factor measurement. Over narrow frequency ranges that repeat quasi-periodically through the spectrum the Y-factor is nearly as good as the “ODC off” reference case. We hypothesise that this is due to a cavity effect between the PAF and the reflector surface resulting in destructive interference of the calibration noise at particular frequencies, meaning that there is significantly less available calibration noise at these frequencies.

Figure 5.7 shows that the calibration noise input adds only 1% to the system temperature on the boresight beam in the “matched” scenario, however outer beams in a `square_6x6` footprint are degraded by up to 9%. This test was performed with the calibration noise set at 2.2 times the single-port system noise power so we should be able to limit worst-case (outer) beam sensitivity degradation to 1% by reducing the calibration noise level to 24% of the single-port system noise. In fact, we plan to set the calibration noise at just 5% of the single-port system noise during astronomical observations and expect beam sensitivity degradation closer to 0.2%.

These measurements and projections should be viewed as upper limits on the degradation of

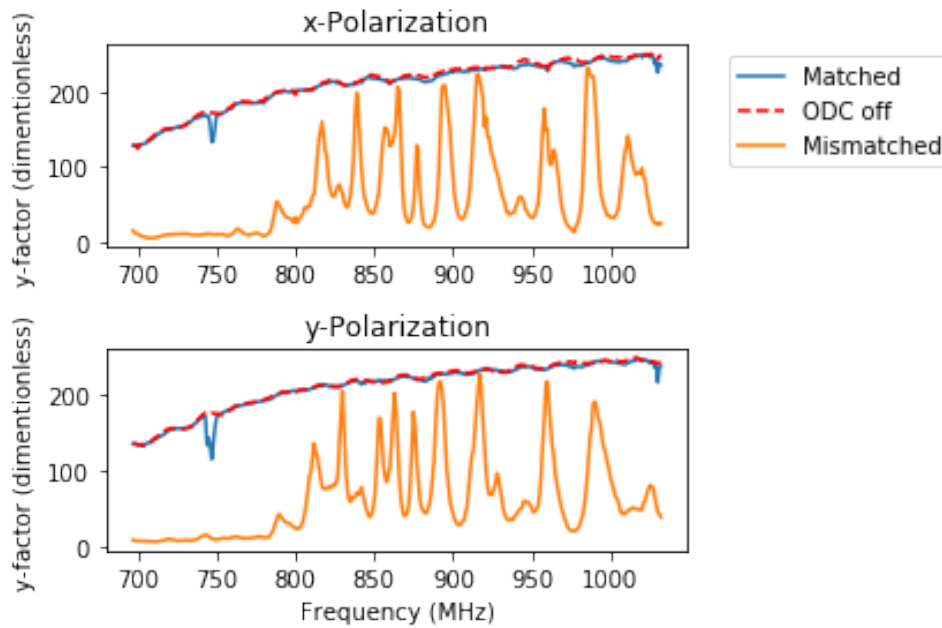


Figure 5.6: Beam sensitivity (Y-Factor) dependence on coordination of beamforming with ODC state. This explores “matched” weights (blue) made and assessed with ODC on, “mismatched” weights (orange) made with ODC off and assessed with ODC on, and a reference “ODC off” case (red) where the ODC was off for both beamforming and sensitivity assessment. When using the ODC it is important for it to be turned on during beamforming.

beam sensitivity. Some of the degradation we measured would have been due to changes in elevation, and thereby spillover, between “matched” and “ODC off” beamformer calibrations. We made multiple measurements of boresight beam degradation with different calibration noise levels over a 15 dB range and always measured an order 1% degradation of the boresight beam.

Finally, Figure 5.8 shows that beamformed sensitivity can be improved a further 3% at lower frequencies by including a returned copy of the calibration noise as one of the beamformer inputs when calculating the maxSNR beamformer weights.

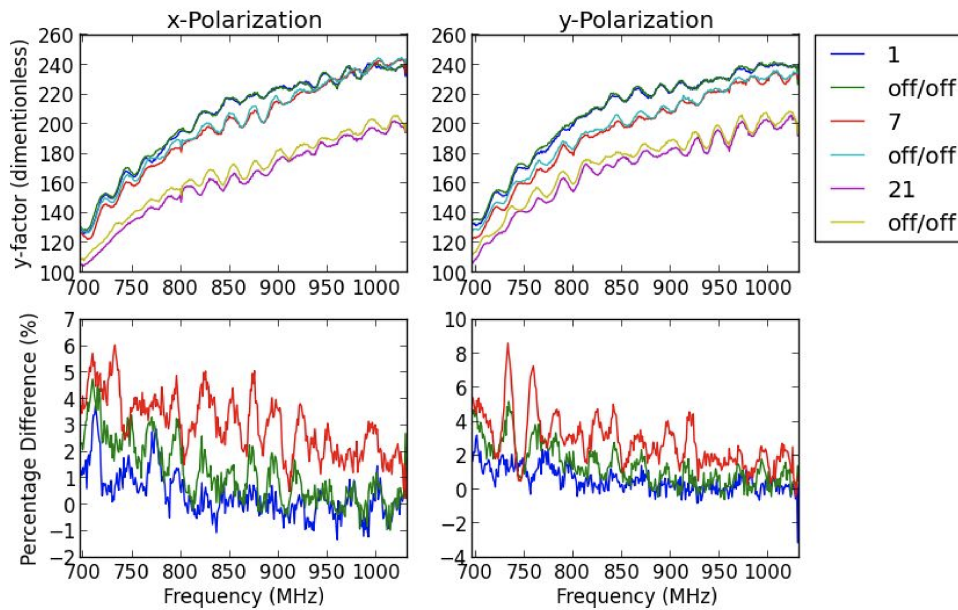


Figure 5.7: The ODC noise has a bigger impact on the sensitivity of outer beams. These plots compare Y-factors for beams 1, 7 and 21 of a `square_6x6` footprint between the “matched” case with the ODC on during beamforming and Y-factor measurement and the reference case where the ODC system was off the whole time.

6 Conclusion and Further Work

Our key finding is that the calibration signal is adequately suppressed in the beamformed output so long as the calibration signal is active when the beamformer weights are calculated. Our measurements suggest that the ODC noise should raise the T_{sys} of beams over the usable FOV by less than 1% so long as the ODC noise is on during beamforming and is no stronger than 24% of the single-port system noise power at the LNA inputs. The calibration signal can be further mitigated below 780 MHz by including a returned copy of the calibration noise as one of the beamformer inputs when calculating the maxSNR beamformer weights.

We have also demonstrated a method of estimating the calibration noise power at the PAF LNA inputs. Plots of this ratio calculated from all PAF ports and frequency channels provide useful diagnostic information about the health of the ODC and PAF systems at the time of measurement. They are also useful when setting the attenuators to equalise the ODC noise level used on all antennas.

Further investigation is required regarding (1) the suspected cavity effect between the reflector and the PAF; (2) why including the calibration noise copy into the beamforming only improves frequencies below approximately 780 MHz; and why the ODC noise has a bigger impact on sensitivity of the outer beams. It appears that the cavity effect is smaller and therefore the electromagnetic relationships between the calibration antenna, the PAF, and the ASKAP antenna are significantly different below 780 MHz. It would also be useful to separate the impact of ODC noise on beam sensitivity from other small and variable noise contributions like spillover.

The next step will be to use the ODC during regular observations in order to calibrate the beam during observations and monitor gain drifts in the PAF electronics.

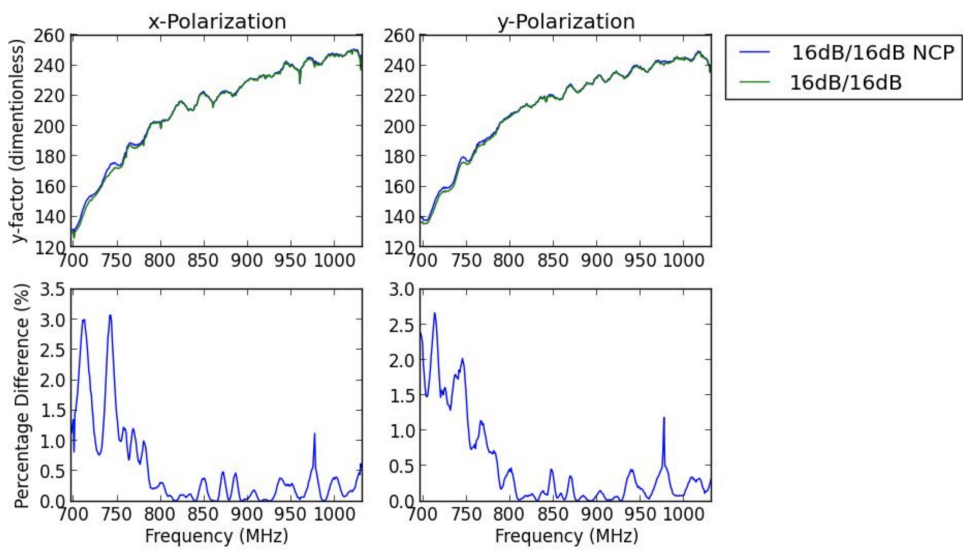


Figure 5.8: Including the calibration port when calculating beam weights improves sensitivity in the lower frequencies up to 3%. The blue trace included a reference copy of the ODC noise source in the maxSNR beamformer weight solution and the green trace did not.

References

- R. Beresford, M Leach, A. P. Chippendale, and D. Hayman. ASKAP on-dish calibration system. In *Phased Array Feed Workshop*, September 2018.
- A. J. Brown, G. A. Hampson, P. Roberts, R. Beresford, J. D. Bunton, W. Cheng, R. Chekkala, D. Kiraly, S. Neuhold, and K. Jeganathan. Design and implementation of the 2nd generation ASKAP digital receiver system. In *2014 International Conference on Electromagnetics in Advanced Applications (ICEAA)*, pages 268–271, August 2014. doi: [10.1109/ICEAA.2014.6903860](https://doi.org/10.1109/ICEAA.2014.6903860).
- J. Dowson. The utility of the ASKAP on-dish calibration system. ACES Memo 17, CSIRO, July 2017. URL <http://www.atnf.csiro.au/projects/askap/ACES-memos>.
- G. A. Hampson, A. Brown, J. D. Bunton, S. Neuhold, R. Chekkala, T. Bateman, and J. Tuthill. ASKAP Redback-3 an agile digital signal processing platform. In *2014 XXXIth URSI General Assembly and Scientific Symposium (URSI GASS)*, pages 1–4, August 2014. doi: [10.1109/URSIGASS.2014.6930062](https://doi.org/10.1109/URSIGASS.2014.6930062).
- D. McConnell et al. The Australian Square Kilometre Array Pathfinder: Performance of the Boolardy Engineering Test Array. *Proc. Astron. Soc. Aust.*, 33:e042, September 2016. doi: [10.1017/pasa.2016.37](https://doi.org/10.1017/pasa.2016.37).

CONTACT US

t 1300 363 400
+61 3 9545 2176
e csiroenquiries@csiro.au
w www.csiro.au

WE DO THE EXTRAORDINARY EVERY DAY

We innovate for tomorrow and help improve today for our customers, all Australians and the world.

Our innovations contribute billions of dollars to the Australian economy every year. As the largest patent holder in the nation, our vast wealth of intellectual property has led to more than 150 spin-off companies.

With more than 5,000 experts and a burning desire to get things done, we are Australia's catalyst for innovation. WE IMAGINE. WE COLLABORATE. WE INNOVATE.

FOR FURTHER INFORMATION

Astronomy and Space Science

Dr. Aaron Chippendale

t +61 2 9372 4296
e Aaron.Chippendale@csiro.au
w www.atnf.csiro.au